NUCLEAR SCIENCE AND ENGINEERING: **164**, 287–303 (2010)

Resonance Parameters and Uncertainties Derived from Epithermal Neutron Capture and Transmission Measurements of Natural Molybdenum

G. Leinweber,* D. P. Barry, J. A. Burke, and N. J. Drindak

Bechtel Marine Propulsion Corporation, Knolls Atomic Power Laboratory
P.O. Box 1072, Schenectady, New York 12301-1072

Y. Danon, R. C. Block, and N. C. Francis

Rensselaer Polytechnic Institute
Department of Mechanical, Aerospace, and Nuclear Engineering
Troy, New York 12180-3590

and

B. E. Moretti

United States Military Academy, Department of Physics
West Point, New York 10996

Received October 27, 2008
Accepted August 7, 2009

Abstract—*The electron linear accelerator facility at the Rensselaer Polytechnic Institute was used to explore neutron interactions with molybdenum in the energy region from 10 eV to 2 keV. Neutron capture and transmission measurements were performed by the time-of-flight technique. Resonance parameters were extracted from the data using the multilevel R-matrix Bayesian code SAMMY. A table of resonance parameters and their uncertainties is presented. Two transmission measurements were performed at a flight path of 25 m with a ^{6}Li glass scintillation detector. The neutron capture measurements were performed at a flight path of 25 m with a 16-segment sodium iodide multiplicity detector. Nine different thicknesses of elemental molybdenum metal samples ranging from 0.051 mm (0.002 in.) to 6.35 mm (0.250 in.) were measured in either capture or transmission. Reductions in resonance integrals were observed when compared to ENDF/B-VII.0 for six of the seven stable isotopes. The largest reductions were 9% in ^{97}Mo and 11% in ^{100}Mo. The one measured increase in resonance integral relative to ENDF/B-VII.0 occurred in ^{95}Mo, and it was significant (10%). The measured distribution of neutron widths for ^{95}Mo and ^{97}Mo are a better match to a Porter-Thomas distribution than those of ENDF/B-VII.0. Neutron strength functions for ^{95}Mo and ^{97}Mo were measured and compared to ENDF/B-VII.0. The strength of ^{95}Mo and ^{97}Mo are within uncertainties of each other. The measured radiation width distribution for ^{95}Mo and ^{97}Mo are compared to those of ENDF/B-VII.0 and to χ^2 distributions. Significant aspects of this analysis are the assignment of radiation widths, the determination of the transmission resolution function, and the propagation of experimental uncertainties into resonance parameter uncertainties.*

I. INTRODUCTION

Molybdenum has many uses in the field of nuclear energy including heat pipes and condenser tubes. It is used in high-strength, low-corrosion stainless steel and other alloys. It can be used in nuclear reactor fuel, especially at a high temperature and in nanoscale reactant particles for superalloys. Thus, its nuclear properties are important for reactor applications.

The purpose of the present work was to determine resonance parameters for elemental molybdenum that are an improvement over the current molybdenum

*E-mail: leinwg@rpi.edu

evaluations. Relevant prior molybdenum measurements include those of Weigmann et al.,[1] Wynchank et al.,[2] and Musgrove et al.[3] Each of these references provided resonance parameters in the energy region below 2 keV. Wasson et al.[4] gave resonance parameters for ^{92}Mo including the two resonances, at 347 and 1860 eV, which are reported here.

The current measurements were made with modern detectors. Data from 10 eV to 2 keV were analyzed with a state-of-the-art R-matrix resonance parameter analysis code, SAMMY (Ref. 5). Because of molybdenum's low thermal cross section (<10 b), thermal data were not taken. The largest resonances occurred at 45 and 131 eV. Both transmission and capture data were employed in the determination of the resonance parameters. Some general information about natural elemental molybdenum is given in Table I. Similarities in binding energy often dictate similar efficiencies for detecting neutron capture gamma rays. Capture detector efficiency is discussed in Secs. II.B and IV.G. The range of previously assigned radiative widths is given in Table I, and it is the most difficult resonance parameter to extract from transmission and capture data. The determination of radiative widths is discussed in Sec. IV.F. All references to ENDF in this paper refer to ENDF/B-VII.0 (Ref. 6) unless explicitly stated otherwise.

II. EXPERIMENTAL CONDITIONS

II.A. Overview

Table II gives some details of the experimental conditions including neutron targets, overlap filters, LINAC pulse repetition rate, flight path length, and channel widths. The neutron energy for a detected event is determined using the time-of-flight (TOF) technique. The nominal resolution of these measurements was 1.8 ns/m for transmission and 3.9 ns/m for capture. Descriptions of the detectors,[7,8] data acquisition,[7,9] and neutron-producing targets[10,11] used in these experiments are available in the references.

Two epithermal transmission measurements and one neutron capture measurement were performed at the electron linear accelerator facility at Rensselaer Polytechnic Institute (RPI). The first transmission experiment was performed in 1995. This experiment was designed to measure the resonance parameters of molybdenum below 200 eV. The second transmission experiment was performed in 2004 and measured resonances up to 2 keV. The measurements included uranium samples used to characterize the resolution function of the detector system. The neutron capture experiment was performed in 1995 to measure resonances up to 600 eV. Above 600 eV scattered neutrons begin to appear in capture data.[12]

Table III lists the sample thicknesses and the measurements made with these samples. The uncertainties in sample thickness were propagated from multiple measurements of sample weight and diameter. The diameter measurements were the dominant component of the uncertainties. All of the samples were elemental metals with the natural abundances given in Table I. All samples were mounted in aluminum sample cans. The thickness of aluminum on each of the front and rear faces of each sample was 0.38 mm. The influence of these sample cans, as well as all background, was measured by including empty sample cans in all measurements. Background in transmission measurements is discussed in Sec. III.B.1.

TABLE I

General Information About Elemental Molybdenum from ENDF

Isotope	Abundance (Atom Fraction)	Binding Energy (MeV)	Minimum Γ_γ ENDF (meV)	Maximum Γ_γ ENDF (meV)	Number of Resonances 10 to 2000 eV	Resonance Energies (eV)
^{92}Mo	0.1484	8.07	304	425	2	347, 1860
^{94}Mo	0.0925	7.37	140	140	1	1500
^{95}Mo	0.1592	9.15	145	310 (all but 1 ≤200) (all but 4 ≤180)	51	See Table IV
^{96}Mo	0.1668	6.82	83	136 (all Γ_γ = 136 meV except at 131 eV)	6	113, 131, 420, 969, 1269, 1498
^{97}Mo	0.0955	8.64	120	225	65	See Table IV
^{98}Mo	0.2413	5.93	71.8	143	9	12, 402, 430, 468, 613, 819, 1124, 1529, 1927
^{100}Mo	0.0963	5.40	46	104	11	97, 364, 507, 536, 787, 1071, 1263, 1407, 1700, 1769, 1941

TABLE II
Molybdenum Experimental Details

Experiment	Overlap Filter	Neutron-Producing Target	Electron Pulse Width (ns)	Average Beam Current (μA)	Beam Energy (MeV)	Energy Region	Channel Width (μs)	Pulse Repetition Rate (pulses/s)	Flight Path Length (m)
Epithermal transmission 2004	Boron carbide	Bare bounce	47	23	52	$E < 38$ eV	0.5	225	25.596
						38 eV $< E <$ 148 eV	0.125		
						$E >$148 eV	0.03125		
Epithermal transmission 1995	Boron carbide	Old bounce	47	26	50	$E < 28$ eV	0.5	250	25.53
						$E >$ 148 eV	0.03125		
Epithermal capture 1995	Boron carbide	Old bounce	100	36	50 to 60	$E < 28$ eV	0.5	200	25.567
						$E >$ 148 eV	0.03125		

II.B. Capture Detector

The capture detector is a gamma detector containing 20 ℓ of NaI(Tl) divided into 16 optically isolated segments.[7–9] The scintillation crystals form an annulus around the neutron beam with the sample at its center. The neutron beam was collimated to a diameter of 4.76 cm. Neutrons that scatter from the sample are absorbed by a 1.0-cm-thick hollow cylindrical liner fabricated of 99.4 wt% ^{10}B carbide ceramic to reduce the number of scattered neutrons reaching the detector. The detector system discriminates against the 478-keV gamma ray from $^{10}\mathrm{B}(n;\alpha,\gamma)$ reactions. The efficiency of the capture detector is ~75% for a single 2-MeV gamma ray. The efficiency of detecting a capture event in molybdenum is close to 100% and varies slightly by isotope and sample thickness. This effect was quantified and described in Sec. IV.G. Reference 7 contains a description of the detector and its signal-processing electronics.

II.C. Transmission Detectors

Neutron transmission measurements were conducted at the 25-m flight station. The 2004 measurement utilized a 12.70-cm (5-in.)-diam, 1.27-cm-thick ^{6}Li glass scintillator housed in a lighttight aluminum box and coupled to two photomultiplier tubes (PMTs) that are out of the neutron beam. The details of this detector design are given in Ref. 13. The measurement with this detector covered the range of incident neutron energies from 10 to 2000 eV. The dead time of the 2004 transmission measurement was 1.8 μs.

The detector used for the 1995 transmission measurement was built by Bicron with a GS-20 lithium glass scintillator containing 6.6% Li enriched to 95% ^{6}Li. The glass was 1.27 cm thick and ~12.7 cm in diameter. It was coupled via a quartz diffuser to a PMT. Data from this detector were limited to 10 to 200 eV because of resolution deterioration due to neutron scattering from the in-beam photomultiplier. The dead time for this measurement was 0.6 μs (Ref. 7). The 1995 measurement is described in Chapter 7 of Ref. 14.

Transmission samples along with empty sample holders, which are used to measure the open-beam count rate, are mounted on an eight-position computer-controlled sample changer. Each data run consists of one complete cycle through the samples, with a predetermined number of LINAC bursts for each sample position. The distribution of bursts per sample position is chosen to minimize the counting statistical error in the measured cross section.[15]

III. DATA REDUCTION

III.A. Capture Data

Neutron capture data-taking and data-reduction techniques at the RPI LINAC are described in Refs. 16 and

TABLE III

Elemental Metal Molybdenum Samples

Nominal Thickness (mm)	Atomic Density (atoms/b)	Uncertainty (atoms/b)	Measurements
0.051	3.088E−04[a]	1E−07	Capture 10 to 600 eV
0.127	7.897E−04	1.6E−06	1995 transmission 10 to 200 eV, capture 10 to 600 eV
0.254	1.642E−03	2E−06	1995 transmission 10 to 200 eV, capture 10 to 600 eV
0.508	3.259E−03	4E−06	Capture 10 to 600 eV
0.635	4.077E−03	4E−06	1995 transmission 10 to 200 eV
1.27	8.160E−03	8E−06	1995 transmission 10 to 200 eV
2.54	1.649E−02	2E−05	1995 transmission 10 to 200 eV, 2004 transmission 10 to 2000 eV
5.08	3.142E−02	3E−05	1995 transmission 10 to 200 eV
6.35	3.958E−02	3E−05	2004 transmission 10 to 2000 eV

[a]Read as 3.088×10^{-4}.

17. For this epithermal measurement of metal samples, background was determined using empty aluminum sample cans.

Processed capture data are expressed as yield. Yield is defined as the number of neutron captures per neutron incident on the sample. Therefore, in addition to the sample data, another set of data was needed to determine the energy profile of the neutron flux. This was done by mounting a 2.54-mm-thick, 97.9 wt% enriched $^{10}B_4C$ sample in the sample changer and adjusting the total energy threshold to record the 478-keV gamma rays from neutron absorption in ^{10}B. These flux data are corrected for transmission through the boron sample. The measured flux was smoothed using a 51-point Savitzky-Golay[18] filter. The smoothed data gave the shape of the flux but not its magnitude. Therefore, the flux was normalized to transmission data as described in Sec. IV.D.

The zero TOF was fitted indirectly through molybdenum resonance energies to the zero TOF in the 2004 transmission measurement.

The capture yield Y_i in TOF channel i was calculated by

$$Y_i = \frac{C_i - B_i}{K\phi_{sm_i}} \quad , \tag{1}$$

where

C_i = dead-time-corrected and monitor-normalized counting rate of the sample measurement

B_i = dead-time-corrected and monitor-normalized background counting rate

K = product of the flux normalization factor and efficiency

ϕ_{sm_i} = smoothed, background-subtracted, and monitor-normalized neutron flux.

This capture yield and its associated statistical uncertainty provided input to the SAMMY data analysis code[5] that extracted the neutron resonance parameters. Systematic components of resonance parameter uncertainties are discussed in Sec. IV.I.

The flux-to-background ratio in the capture experiment rises from 180 at 12 eV to 320 at 45 eV, and to 400 at 100 eV. The flux-to-background ratio then remains constant at about 400-to-1 out to 600 eV. The flux-to-background ratio is worse at low energies because of absorption in the $1/v$ cross section of the boron overlap filter.

III.B. Transmission Data

The transmission, which is approximately the ratio of the count rate with a sample in the beam to the count rate with samples removed, is given by Eq. (2):

$$T_i = \frac{(C_i^S - K_S B_i - B_S)}{(C_i^O - K_O B_i - B_O)} \quad , \tag{2}$$

where

T_i = transmission in TOF channel i

C_i^S, C_i^O = dead-time-corrected and monitor-normalized counting rates of the sample and open measurements in channel i, respectively

B_i = unnormalized, time-dependent background counting rate in channel i

B_S, B_O = steady-state background counting rates for sample and open measurements, respectively

K_S, K_O = normalization factors for the sample and open background measurements.

The zero TOF was determined by fitting ^{238}U resonances from a depleted uranium sample included in the 2004 transmission measurement.

III.B.1. Transmission Background

The 2004 transmission measurement consisted of two molybdenum samples (2.54 and 6.35 mm), two depleted uranium samples, 13.2 and 4.83 mm, and the open beam. A 6.35-mm-thick sodium filter was placed in the beam throughout the measurement. This filter leaves a notch in the TOF spectrum by removing neutrons scattered by the strong 2.8-keV resonance, which was used to normalize the TOF-dependent background. The TOF-dependent background in the molybdenum data was determined from three saturated resonances. Those resonances are at 45 and 131 eV in molybdenum, and the fixed sodium notch is at 2.8 keV. The open-beam background was assumed to have the same functional shape as the molybdenum background. It was normalized to the background at the fixed sodium notch at 2.8 keV, which was in place for all open-beam measurements.

The TOF-dependent background for the two uranium samples in the 2004 measurement was fitted from five saturated resonances. They were at ~6, 21, 36, and 190 eV in uranium plus the fixed sodium notch at 2.8 keV. The uranium data provide information about the flight path, time zero, and resolution function.

The background determination for the 1995 transmission measurement is described in Ref. 14.

The signal-to-background ratio for the 2004 transmission measurement was 10 at 10 eV, 16 at 45 eV, and 18 at 100 eV. The ratio remained constant at 18 up to 2000 eV. The signal-to-background ratio for the 1995 transmission measurement was 4 at 20 eV, 16 at 45 eV, peaked at 32 at 110 eV, and gradually decreased to 28 at 200 eV. Reference 14 describes the determination of the time-dependent background for the 1995 transmission measurement.

IV. RESULTS

IV.A. Resonance Parameters

Resonance parameters, neutron width Γ_n, radiation width Γ_γ, and resonance energy E, were extracted from the capture and transmission data sets using the SAMMY version 7 multilevel R-matrix Bayesian code.[5] This was a combined transmission and capture analysis, which employed the experimental resolution and Doppler-broadening, self-shielding, and multiple-scattering features of SAMMY. The resulting resonance parameters of natural molybdenum are listed in Table IV. In Table IV resonance parameters and their uncertainties are given

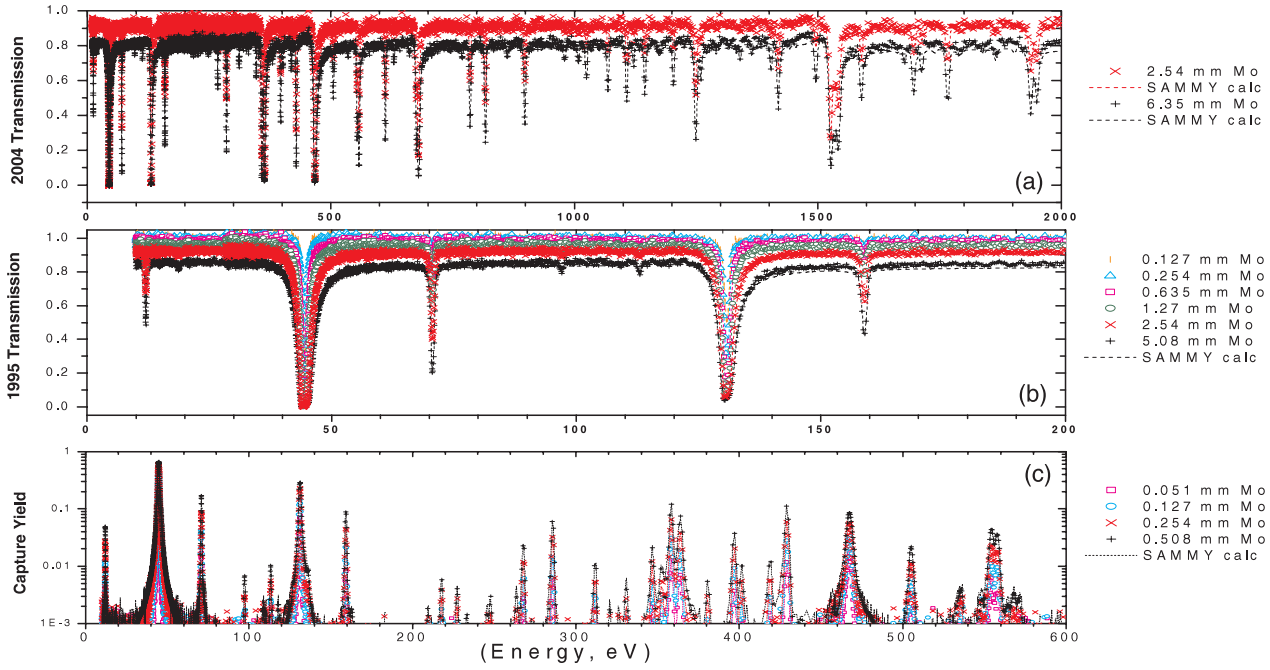

Fig. 1. Overview of all of the data that were analyzed. Neutron transmission and capture data, and SAMMY fits. Data from three experiments utilizing 12 sample thicknesses were analyzed. Resonance parameters are given in Table IV. (a) Molybdenum transmission data taken in 2004. (b) Molybdenum transmission data taken in 1995 whose analysis ends at 200 eV where the resolution function has been characterized. (c) Neutron capture yield data whose analysis ends at 600 eV where contamination from scattered neutrons is minimal.

TABLE IV

Resonance Parameters for Molybdenum Compared with ENDF/B-VII.0 Parameters

E (eV) ΔE (eV)	E_{ENDF} (eV)	Γ_γ (meV) $\Delta\Gamma_\gamma$ (meV)	Γ_γ Source	$\Gamma_{\gamma,ENDF}$ (meV)	Γ_n (meV) $\Delta\Gamma_n$ (meV)	$\Gamma_{n,ENDF}$ (meV)	A	l	πJ
12.070 ± 0.001	12.10	120 ± 30	AVG	120	0.0309 ± 0.0002	0.029	98	p	−1.5
44.644 ± 0.001	44.90	181.9 ± 0.7	FIT	150	173.7 ± 0.4	171.429	95	s	3.0
70.839 ± 0.001	70.92	140 ± 20	AVG	130	18.86 ± 0.07	20.160	97	s	2.0
79.5 ± 0.1	79.55		ENDF	120	0.16 ± 0.05	0.220	97	p	−1.0
97.34 ± 0.02	97.20	69 ± 7	AVG	80	0.17 ± 0.01	0.180	100	p	−1.5
108.5 ± 0.1	108.80		ENDF	188	0.11 ± 0.03	0.160	94	p	−0.5
109.2 ± 0.1	109.58		ENDF	210	0.37 ± 0.10	0.440	97	p	−1.0
110.2 ± 0.1	110.40		ENDF	310	0.25 ± 0.06	0.320	95	p	−1.0
113.29 ± 0.02	113.40		ENDF	136	0.42 ± 0.02	0.451	96	p	−0.5
117.87 ± 0.08	117.80		ENDF	200	0.21 ± 0.03	0.180	95	p	−2.0
127.01 ± 0.10	126.89		ENDF	210	0.52 ± 0.09	0.400	97	p	−1.0
131.171 ± 0.002	131.40	85.4 ± 0.4	FIT	83	259.8 ± 0.6	326.000	96	s	0.5
136.22 ± 0.05	136.32		ENDF	210	0.45 ± 0.05	0.800	97	p	−4.0
159.365 ± 0.005	159.50	170 ± 40	AVG	166	13.82 ± 0.10	12.857	95	s	3.0
209.5 ± 0.2	209.98		ENDF	210	0.5 ± 0.1	0.733	97	p	−4.0
217.88 ± 0.05	217.90		ENDF	180	1.02 ± 0.09	0.867	95	p	−4.0
227.42 ± 0.08	227.58		ENDF	210	1.7 ± 0.2	2.057	97	p	−3.0
233.3 ± 0.2	233.33		ENDF	210	0.6 ± 0.1	0.566	97	p	−3.0
245.7 ± 0.2	245.80		ENDF	180	0.6 ± 0.2	0.600	95	p	−2.0
248.0 ± 0.1	247.91		ENDF	210	1.1 ± 0.2	1.067	97	p	−4.0
263.6 ± 0.1	263.80		ENDF	180	0.9 ± 0.2	1.200	95	p	−3.0
267.90 ± 0.01	268.02	120 ± 30	AVG	162	14.7 ± 0.3	14.571	97	s	3.0
285.855 ± 0.006	286.03	135 ± 6	FIT	162	105 ± 1	72.000	97	s	2.0
311.77 ± 0.04	312.07	120 ± 30	AVG	162	8.6 ± 0.4	8.571	97	s	3.0
320.9 ± 0.2	321.12		ENDF	210	1.1 ± 0.3	1.267	97	p	−4.0
330.8 ± 0.1	331.40		ENDF	180	1.5 ± 0.2	2.267	95	p	−4.0
346.87 ± 0.03	347.00		ENDF	304	7.6 ± 0.3	7.900	92	s	0.5
352.54 ± 0.05	352.71		ENDF	210	8.6 ± 0.6	7.714	97	p	−3.0
358.420 ± 0.005	358.30	150 ± 2	FIT	145	222 ± 2	274.286	95	s	3.0
363.924 ± 0.006	363.70	56 ± 1	FIT	70	604 ± 3	640.000	100	s	0.5
380.79 ± 0.10	380.91		ENDF	210	5.9 ± 0.6	5.143	97	p	−3.0
396.99 ± 0.01	397.16	140 ± 10	FIT	162	70 ± 1	64.286	97	s	3.0
401.44 ± 0.05	402.00	120 ± 30	AVG	120	1.38 ± 0.08	1.620	98	p	−1.5
417.4 ± 0.5	418.20		ENDF	180	1.2 ± 0.5	1.200	95	p	−2.0
419.06 ± 0.05	420.00		ENDF	136	5.9 ± 0.3	6.060	96	p	−0.5
429.203 ± 0.007	430.00	113 ± 5	FIT	123	67.5 ± 0.8	73.400	98	p	−0.5
457.5 ± 0.3	457.30		ENDF	210	2.2 ± 0.5	2.040	97	p	−2.0
467.454 ± 0.007	468.00	88.5 ± 0.7	FIT	96	782 ± 3	759.000	98	s	0.5
	469.70		ENDF	180		9.4285	95	p	−3.0
505.09 ± 0.03	505.45	160 ± 20	FIT	162	75 ± 2	74.400	97	s	2.0
506.65 ± 0.04	507.40	90 ± 50	AVG	80	4.0 ± 0.9	4.400	100	p	−0.5
528.9 ± 0.7	528.34		ENDF	210	1.2 ± 0.6	1.286	97	p	−3.0
533.7 ± 0.4	533.81		ENDF	210	3.5 ± 1.0	3.857	97	p	−3.0
535.8 ± 0.2	536.10	90 ± 50	AVG	80	4.2 ± 0.6	4.200	100	p	−0.5
548.3 ± 0.2	548.25		ENDF	210	4.3 ± 0.7	3.857	97	p	−3.0
554.29 ± 0.01	554.40	182 ± 6	FIT	150	146 ± 2	132.000	95	s	2.0
557.83 ± 0.01	558.43	119 ± 3	FIT	152	473 ± 5	514.286	97	s	3.0
564.1 ± 0.6	564.06		ENDF	210	2.2 ± 0.8	2.229	97	p	−3.0
568.0 ± 0.3	568.00		ENDF	210	5 ± 1	5.743	97	p	−3.0
571.2 ± 0.2	571.97		ENDF	210	7 ± 2	6.720	97	p	−2.0
579.5 ± 0.8	578.52		ENDF	210	1.1 ± 0.5	1.133	97	p	−4.0
596.7 ± 0.8	595.70		ENDF	180	0.7 ± 0.3	0.720	95	p	−3.0
612.25 ± 0.09	613.00	120 ± 10	FIT	143	60 ± 1	65.800	98	p	−0.5
629.7 ± 0.1	630.00		ENDF	180	20 ± 2	24.000	95	p	−2.0

(Continued)

TABLE IV (Continued)

E (eV)	ΔE (eV)	E_{ENDF} (eV)	Γ_γ (meV)	$\Delta\Gamma_\gamma$ (meV)	Γ_γ Source	$\Gamma_{\gamma,ENDF}$ (meV)	Γ_n (meV)	$\Delta\Gamma_n$ (meV)	$\Gamma_{n,ENDF}$ (meV)	A	l	πJ
653.1	0.6	653.16			ENDF	210	2.0	0.8	1.800	97	p	−4.0
661.4	0.2	661.60	170	40	AVG	150	9	1	15.429	95	s	3.0
675.70	0.03	676.32	220	50	FIT	225	312	7	330.000	97	s	3.0
680.37	0.02	680.70	210	40	FIT	145	900	20	711.429	95	s	3.0
694.4	0.4	694.68			ENDF	210	11	3	15.000	97	p	−2.0
699.4	0.5	700.74			ENDF	210	5	2	6.200	97	p	−4.0
700.7	0.7	702.80			ENDF	180	2.0	0.9	2.486	95	p	−3.0
708.2	0.3	708.30			ENDF	180	4.9	0.9	8.933	95	p	−4.0
745.4	0.5	745.50			ENDF	180	8	3	11.000	95	p	−1.0
769.9	0.2	769.80	170	40	AVG	150	14	1	24.000	95	s	3.0
784.1	0.6	787.40	90	50	AVG	80	5	3	5.800	100	p	−0.5
786.03	0.04	786.48	120	30	AVG	162	300	7	402.857	97	s	3.0
809.6	0.9	809.20			ENDF	210	4	2	4.800	97	p	−2.0
817.76	0.03	819.00	120	30	FIT	103	59	1	68.000	98	p	−1.5
862.5	0.2	862.50	140	20	AVG	162	38	4	61.920	97	s	2.0
898.65	0.05	898.40	140	50	FIT	175	321	6	318.000	95	s	2.0
906.3	0.7	905.68			ENDF	210	7	2	6.667	97	p	−4.0
932	1	932.10			ENDF	180	5	3	7.000	95	p	−1.0
954	1	956.50			ENDF	180	3	1	3.000	95	p	−1.0
968.4	0.8	969.00			ENDF	136	2.4	0.9	2.750	96	p	−0.5
976.0	0.8	975.14			ENDF	210	13	4	17.040	97	p	−2.0
980.7	0.2	980.70	180	10	AVG	150	36	4	44.400	95	s	2.0
1008.5	0.3	1008.2	140	20	AVG	162	60	20	84.000	97	s	2.0
1008.9	0.5	1011.1			ENDF	180	8	4	8.400	95	p	−4.0
1024.8	0.1	1025.0	170	40	AVG	150	80	4	94.286	95	s	3.0
1036.1	0.5	1035.7			ENDF	180	7	2	8.800	95	p	−4.0
1051.3	0.7	1051.7			ENDF	188	6	2	6.100	94	p	−0.5
1062.8	0.8	1059.2			ENDF	180	5	2	7.886	95	p	−3.0
1069.17	0.10	1070.7	70	40	FIT	104	64	2	65.000	100	p	−1.5
1107.87	0.10	1108.7	120	70	FIT	137	470	10	336.000	97	s	2.0
1122	1	1122.5			ENDF	180	3	1	2.667	95	p	−4.0
1122.2	0.2	1124.0	120	30	AVG	120	9.5	0.8	10.400	98	p	−1.5
1133.7	0.6	1133.4	140	20	AVG	162	22	6	73.440	97	s	2.0
1145.0	0.1	1144.6	160	80	FIT	173	224	8	300.000	95	s	2.0
1173.2	0.5	1170.5			ENDF	180	11	3	13.733	95	p	−4.0
1176.7	0.5	1176.4	140	20	AVG	162	52	9	109.200	97	s	2.0
		1194.2			ENDF	210			6.333	97	p	−4.0
1203.7	0.1	1203.4	140	70	FIT	150	144	6	112.286	95	s	3.0
1249.6	0.1	1248.8	130	60	FIT	150	1240	20	454.286	97	s	3.0
1260.4	0.2	1263.0	69	7	AVG	89	47	3	50.000	100	p	−1.5
1271	1	1269.0			ENDF	136	1.1	0.5	2.240	96	p	−0.5
1271.6	0.7	1270.4	120	30	AVG	162	20	5	50.229	97	s	3.0
1290.9	0.4	1293.1	120	30	AVG	162	21	8	37.286	97	s	3.0
1293	1	1296.9			ENDF	180	8	4	9.429	95	p	−3.0
1319	1	1317.6	140	20	AVG	162	19	7	77.160	97	s	2.0
1333.4	0.5	1333.5			ENDF	210	26	8	36.667	97	p	−4.0
1340.9	0.3	1340.7			ENDF	180	49	6	39.429	95	p	−3.0
1364	2	1360.6			ENDF	180	7	3	7.200	95	p	−2.0
1365.0	0.5	1364.3	120	30	AVG	162	48	8	65.143	97	s	3.0
1375.6	0.6	1375.4			ENDF	210	13	6	9.771	97	p	−3.0
1384.6	0.2	1386.7			ENDF	180	9	4	9.943	95	p	−3.0
1398.6	0.7	1398.0			ENDF	210	11	5	12.000	97	p	−3.0
1404.3	0.2	1407.4	56	1	AVG	46	107	7	116.000	100	s	0.5
1418.7	0.2	1419.3	140	70	FIT	146	420	20	531.429	95	s	3.0
1423.4	0.5	1425.2	120	30	AVG	162	50	10	111.429	97	s	3.0

(Continued)

TABLE IV (Continued)

E (eV)	ΔE (eV)	E_{ENDF} (eV)	Γ_γ (meV)	$\Delta\Gamma_\gamma$ (meV)	Γ_γ Source	$\Gamma_{\gamma,ENDF}$ (meV)	Γ_n (meV)	$\Delta\Gamma_n$ (meV)	$\Gamma_{n,ENDF}$ (meV)	A	l	πJ
1441	± 1	1437.0			ENDF	180	8	± 3	13.371	95	p	−3.0
		1453.1			ENDF	210			12.533	97	p	−4.0
1493	± 2	1485.0			ENDF	210	10	± 4	10.114	97	p	−3.0
1496.1	± 0.2	1495.5	180	± 10	AVG	150	330	± 20	102.000	95	s	2.0
1498.4	± 0.3	1498.0			ENDF	136	10	± 5	10.100	96	p	−0.5
1526.4	± 0.2	1529.0	70	± 30	FIT	71.8	1390	± 30	1280.000	98	s	0.5
1534.8	± 0.2	1534.2	150	± 70	FIT	150	1570	± 60	498.000	97	s	2.0
1542.4	± 0.2	1541.8	140	± 60	FIT	140	1420	± 30	1100.000	94	s	0.5
1553	± 2	1554.2			ENDF	210	12	± 5	11.600	97	p	−1.0
		1570.0			ENDF	180			10.2857	95	p	−3.0
1575.2	± 0.6	1576.8			ENDF	180	9	± 4	8.914	95	p	−3.0
1589.6	± 0.2	1589.5	180	± 90	FIT	188	360	± 10	245.143	95	s	3.0
1597.3	± 0.2	1596.4	140	± 20	AVG	120	70	± 20	216.000	97	s	2.0
1630	± 2	1628.4			ENDF	210	8	± 4	17.280	97	p	−2.0
1664	± 1	1660.4			ENDF	188	6	± 2	6.200	94	p	−1.5
1677.6	± 0.4	1677.4	180	± 10	AVG	150	120	± 10	120.000	95	s	2.0
1695.4	± 0.4	1699.0	160	± 20	FIT	162	110	± 10	114.857	97	s	3.0
1697.5	± 0.3	1700.4	69	± 7	FIT	69	150	± 10	180.000	100	p	−1.5
		1704.1			ENDF	180			36.7	95	p	−3.0
1713.0	± 0.3	1712.5	140	± 20	AVG	162	390	± 30	252.000	97	s	2.0
		1740.7			ENDF	210			24.800	97	p	−4.0
1766.2	± 0.4	1766.1	190	± 90	FIT	183	330	± 80	348.857	95	s	3.0
1767.9	± 0.4	1769.5	90	± 50	FIT	89	220	± 60	21.000	100	p	−0.5
1789.1	± 0.5	1788.0			ENDF	180	40	± 20	74.400	95	p	−2.0
1795.5	± 0.3	1795.0			ENDF	210	30	± 10	36.067	97	p	−4.0
1834	± 2	1835.9			ENDF	210	12	± 5	11.743	97	p	−3.0
1842	± 1	1841.7			ENDF	180	24	± 7	25.867	95	p	−4.0
		1853.3			ENDF	180			4.2667	95	p	−4.0
1864.8	± 0.8	1860.0			ENDF	425	22	± 4	23.800	92	p	−1.5
1868	± 2	1865.0			ENDF	210	12	± 5	12.000	97	p	−4.0
1868	± 2	1870.9			ENDF	210	40	± 20	36.000	97	p	−1.0
		1903.8			ENDF	210			54.000	97	p	−4.0
1921	± 1	1925.1			ENDF	180	18	± 2	30.857	95	p	−3.0
1927.5	± 0.3	1927.0	120	± 30	AVG	120	11	± 4	11.000	98	p	−1.5
1934	± 1	1931.5	140	± 20	AVG	162	50	± 20	219.600	97	s	2.0
1937.3	± 0.3	1941.1	60	± 30	FIT	56	920	± 40	1010.000	100	s	0.5
1942.8	± 0.3	1940.8	120	± 30	AVG	162	40	± 20	214.286	97	s	3.0
1949.7	± 0.3	1950.2	170	± 90	FIT	172	910	± 30	468.000	95	s	2.0
1959.5	± 0.4	1961.3			ENDF	180	18	± 10	18.400	95	p	−4.0

and compared to ENDF/B-VII.0. The column labeled "A" (the 11th column in Table IV) gives the atomic number for the isotope containing the resonance. The column labeled "l" (the 12th column in Table IV) gives the angular momentum state of the resonance, s-wave or p-wave. Some small resonances were not fitted, and their parameters are listed for ENDF/B-VII only.

Three experiments were performed to resolve molybdenum resonances between 10 eV and 2 keV as described in Sec. II.A. An overview of the results is shown in Fig. 1. Figure 1 shows data and calculated curves, using SAMMY. It illustrates the level structure and the multiple experiments and sample thicknesses used to determine the resonance parameters. Overall, 12 samples were measured in transmission and capture. The 1995 transmission measurement utilizing "thin" molybdenum samples was analyzed only between 10 and 200 eV where the resolution function was fitted and the thin samples were well suited to this region of strong molybdenum resonances.[14]

The two strongest, low-energy resonances of molybdenum occur at 45 and 131 eV. The latter is shown in Fig. 2. The resonance is narrower than suggested by ENDF. ENDF/B-VI.8 was a slightly better match than ENDF/B-VII.0.

Both capture and transmission data have been fitted to a single set of resonance parameters in the region

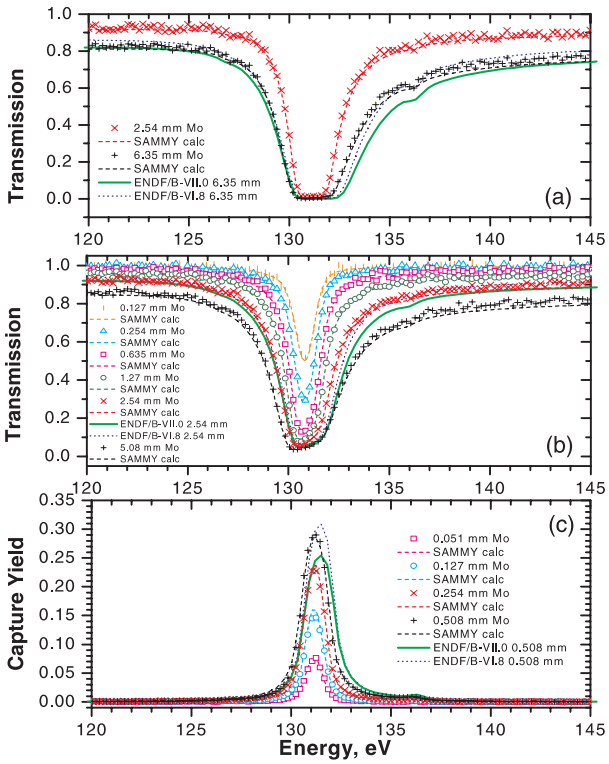

Fig. 2. Experimental data near the 131-eV resonance in molybdenum. (a) Molybdenum transmission data taken in 2004. (b) Molybdenum transmission data taken in 1995. (c) Neutron capture yield data. The resonance is narrower than suggested by ENDF. ENDF/B-VI.8 was a slightly better match to the data than ENDF/B-VII.

below 600 eV. Neutron capture data were analyzed only below 600 eV to minimize the effect of scattered neutrons getting captured in the sodium iodide. The Monte Carlo–calculated fraction of scattered neutrons that penetrate the liner and enter into the NaI is ~5% at 600 eV (Ref. 12). An example of the fits in this region is given in Fig. 3 for the 360-eV doublet. The second resonance of the doublet is narrower than suggested by ENDF. Another example is given in Fig. 4 for the 467-eV resonance. In this strong resonance the measured resonance widths are minor modifications from ENDF/B-VII.0. However, the measured resonance energy agrees better with ENDF/B-VI.8.

In the 600 to 2000 eV energy region, resonance parameters were fitted exclusively to the two thick molybdenum samples, 2.54 and 6.35 mm thick, measured in transmission in 2004. Thick uranium samples, 13.2 and 4.83 mm thick, were included in the measurement to determine the resolution function, time zero, and flight path length.

Improvements to resonance parameters were evident throughout the energy spectrum. The 2004 molybdenum transmission data in the region of the 1255-eV doublet are shown in Fig. 5. The first resonance in the doublet is stronger than suggested by ENDF. The second resonance is a refinement of the ENDF/B-VII resonance parameters. Our measurements confirm the existence of the molybdenum resonance at ~1404 eV, which is included in ENDF/B-VII.0 but not in ENDF/B-VI.8. A triplet of resonances at 1535 eV is shown in Fig. 6. This region is an excellent example

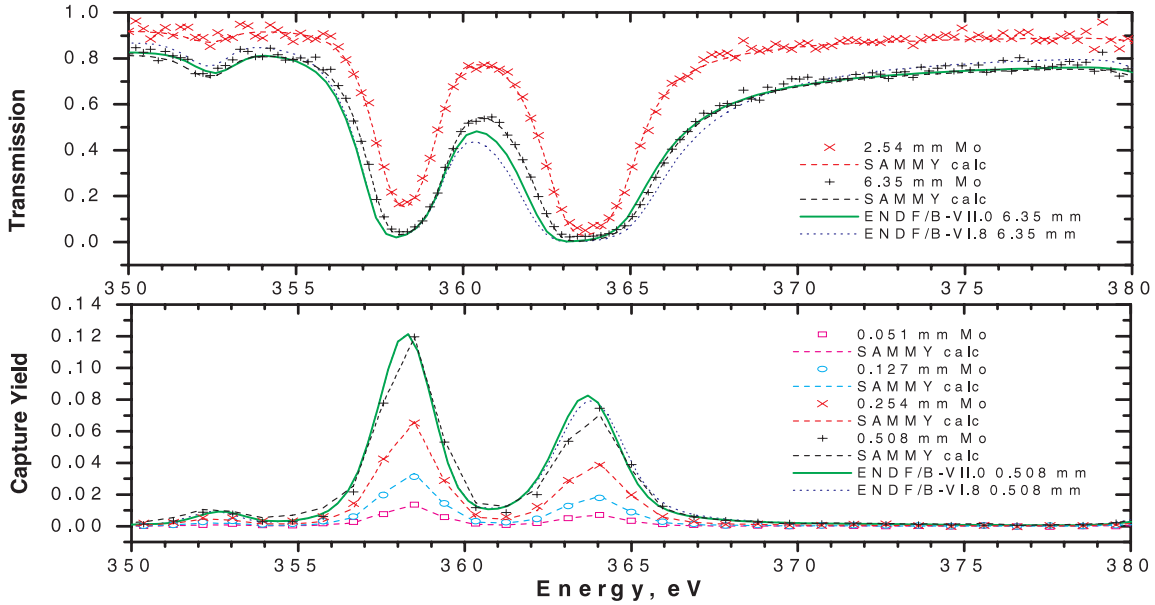

Fig. 3. Experimental data near the 360-eV doublet in molybdenum. The 358-eV resonance ENDF/B-VII resonance parameters are unchanged from ENDF/B-VI.8. The second resonance of the doublet is narrower than suggested by ENDF. The RPI resonance parameters were a result of a combined fit to all the data sets shown here.

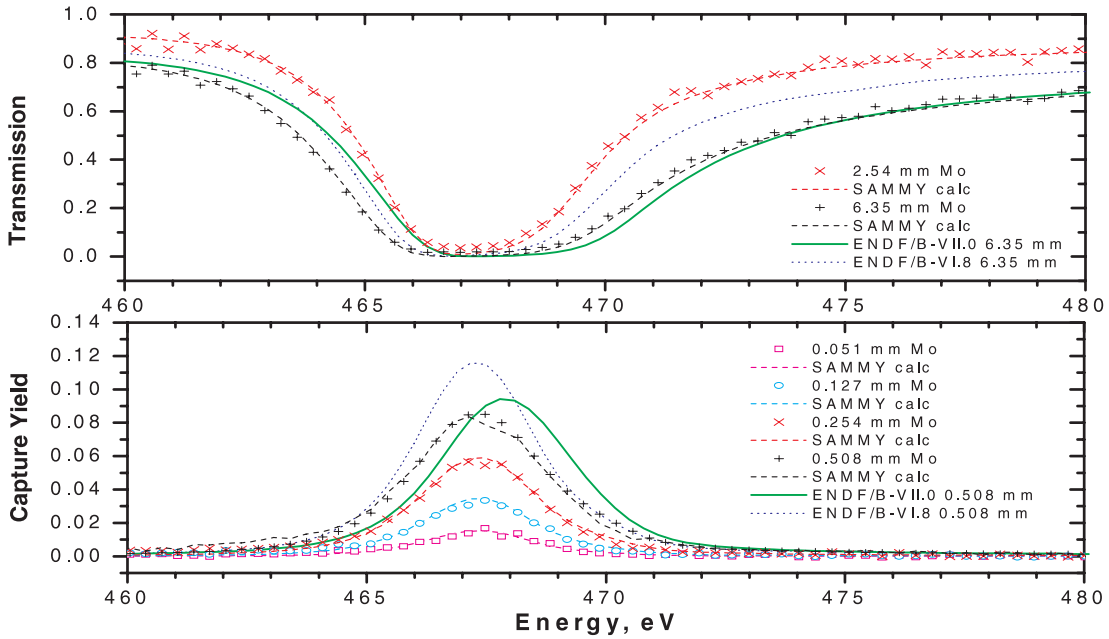

Fig. 4. Experimental data near the 467-eV resonance in molybdenum. ENDF/B-VII.0 appears to be an improvement over ENDF/B-VI.8 in terms of resonance widths. However, ENDF/B-VI.8 made a better match to the resonance energy.

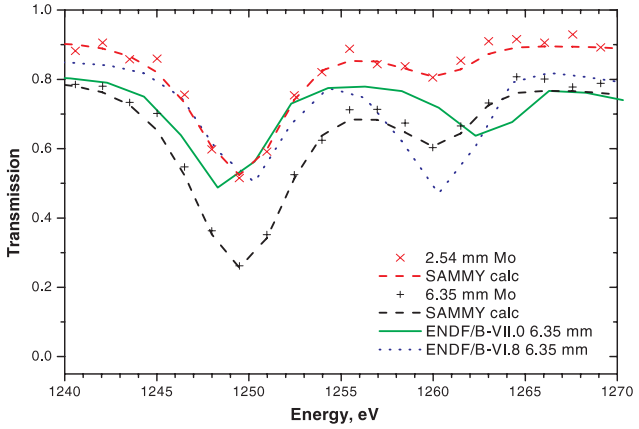

Fig. 5. 2004 molybdenum transmission data in the region of the 1255-eV doublet. The first resonance in the doublet is stronger than suggested by ENDF. The second resonance is a refinement of the ENDF/B-VII.0 resonance parameters. The two ENDF curves correspond to the 6.35-mm Mo thickness. Yet the ENDF curves lie closer to the thin sample data near the 1249.6-eV resonance. The 6.35-mm Mo data and the corresponding SAMMY fit display a larger neutron width. This resonance and the one at 1534.8 eV, shown in Fig. 6, are the primary reason why the ^{97}Mo neutron strength function shown in Table VIII is larger than that of ENDF/B-VII.0.

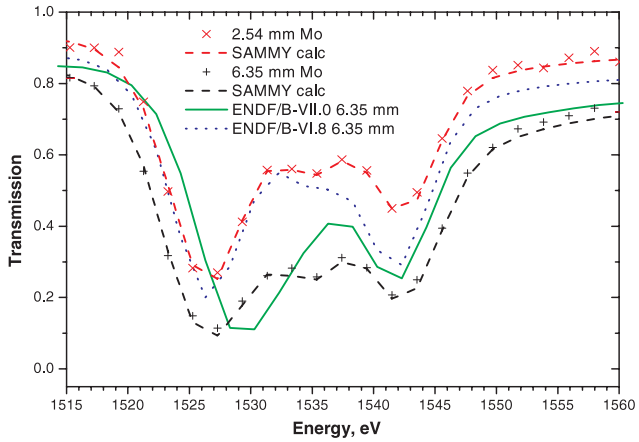

Fig. 6. 2004 molybdenum transmission data in the region of 1535 eV. There are three resonances between 1525 and 1545 eV. The SAMMY curve is a much better fit to the data than ENDF because the middle resonance at 1534.8 eV is much stronger relative to ENDF. This resonance contributes to the larger ^{97}Mo neutron strength function shown in Table VIII.

of where width assignments of overlapping resonances were improved over those of ENDF/B-VII. This triplet has a different set of widths than those given by ENDF.

IV.B. Details of the SAMMY Analysis

Energy regions over which each sample has been fitted are given in Table III. Thin samples were measured in 1995 to characterize the strong resonances below 200 eV. The 2004 measurement used thick molybdenum samples to emphasize the smaller resonances

up to 2000 eV. Two thick uranium samples were also included in the 2004 measurement to characterize the transmission resolution function, which is more important at high energies.

Background was not fitted during the SAMMY analysis. Background was accounted for in the data processing (see Sec. III) of each sample's counting spectrum before they were divided into transmission and capture yield. Normalization was not varied in transmission fits. Capture normalization was fitted to transmission data using the method described in Sec. IV.D.

The present measurements assumed the same spin assignments as ENDF/B-VII.0 for all resonances analyzed. Resonance parameters of the two bound level resonances of Mo were not varied. The temperature used in the fits was 293 K, and no external R-function was employed. Distant resonances were represented by including all of the resonances present in the ENDF file.

All of the molybdenum samples were produced from the same batch of material. The impurities are listed in Table V. The only significant contaminant in the samples was tungsten. The quantity of elemental tungsten was fit to the 18.8-eV resonance in the thickest molybdenum samples. The resulting abundance was 61 ppm tungsten. The other impurities listed in Table V were identified by chemical analysis. Only the tungsten content was included in the SAMMY analysis.

IV.C. Nuclear Radii

The nuclear radii used in the present analysis for molybdenum are taken from ENDF/B-VII. ENDF/B-VII nuclear radii fit the transmission data between resonances significantly better than those in ENDF/B-VI.8.

The radii that were used for penetrabilities and phase shifts were calculated using Eq. (3) (Refs. 5 and 6):

$$a = 1.23 \times AWRI^{1/3} + 0.8 \ , \qquad (3)$$

where a is in fm, and $AWRI$ is the ratio of the atomic weight to the mass of the neutron.

When the nuclear radii of molybdenum were fitted to the 6.35-mm-thick molybdenum transmission data, the resulting nuclear radii were not statistically significantly different from ENDF/B-VII.

TABLE V

Impurities in the Molybdenum Samples

Impurity	ppm	Impurity	ppm
W	61	Mg	<10
C	20	Mn	<10
Fe	14	Ni	<10
Al	<10	Pb	<10
Ca	<10	Si	<10
Cr	<10	Sn	<10
Cu	<10	Ti	<10

IV.D. Capture Flux Normalization

The neutron flux measurement for the capture experiment was described in Sec. III.A. The flux was normalized to all of the 2004 transmission data using the following procedure:

1. Molybdenum neutron widths were fitted to all of the transmission data. Radiation widths were fixed to ENDF/B-VII.0 values.

2. Capture yield normalization was fitted using the transmission-derived neutron widths for all resonances between 10 and 600 eV.

3. Molybdenum resonance parameters were fitted to both transmission and capture data.

This iterative process converged on the set of resonance parameters and the capture flux normalization.

IV.E. Resolution Function

Resolution broadening refers to the combined effects of the LINAC electron burst width, the mean free path of a neutron in the moderator, the TOF channel width, and the effect of the detector system. The resolution function was characterized in SAMMY as a Gaussian distribution in time plus an exponential tail. The width of the electron burst and the channel widths are given in Table II. The width of the exponential tail of the distribution was fitted to be 60 ns from depleted uranium capture measurements.[13] For transmission the width of the exponential tail was fitted to the two depleted uranium samples (4.83 and 13.2 mm thick) included in the 2004 transmission measurement. The width varied from 90 ns at 100 eV to 30 ns at 2 keV. This variable exponential width was included in all SAMMY fits to molybdenum transmission. The flight path for the 2004 transmission measurement was fitted to the two depleted uranium samples and found to be 25.596 ± 0.007 m. The capture flight path length was indirectly derived from the 2004 depleted uranium transmission data. The capture flight path length was fitted to transmission-derived molybdenum resonances. The capture flight path length was 25.58 ± 0.02 m. The 1995 transmission measurement utilized the RPI resolution function option in SAMMY. The burst width and channel width components of the resolution function used in the analysis of the 1995 RPI transmission measurement are given in Table II. The detector used in that measurement, a single-PMT in-beam ^{6}Li glass detector, is described in Table B.1.1 of Ref. 19.

IV.F. Radiation Width Determination

For very low-energy resonances, where the resolution width is minimal, the radiation width can be derived

directly from the measured width of the resonance. At higher energy, radiation widths can be determined whenever a resonance includes a significant quantity of scattering. A criterion of $\Gamma_\gamma/\Gamma_n < 5$ was chosen in Ref. 13 to reflect sensitivity of a resonance to the value of the radiation width. Whenever $\Gamma_\gamma/\Gamma_n < 5$, radiation widths were extracted from the transmission and capture data. But, for resonances whose Γ_γ/Γ_n ratio was greater than five, both measurements effectively measure the same quantity, Γ_n. For these mostly capture resonances, neither transmission nor capture data contain sufficient radiation width information. These resonances were assigned an average radiation width, which was determined in the following way.

Resonances sensitive to the value of the radiation width were identified for each isotope, orbital angular momentum, and where data were available, spin (total angular momentum). Resonances were chosen to use in the determination of the average radiation width $\langle\Gamma_\gamma\rangle$ if they met all of the following criteria:

1. The capture-to-scattering ratio Γ_γ/Γ_n was <5.

2. Thin and thick transmission data or transmission and capture data were taken at the resonance energy.

3. The resonance was not a minor member of a multiplet, i.e., a shoulder on a larger resonance.

Each $\langle\Gamma_\gamma\rangle$ was an inverse-variance-weighted average radiation width.

The radiation widths and uncertainties in Table IV were taken directly from the combined transmission and capture fit using SAMMY with the following exception: If a resonance did not meet all of the three criteria listed above and an $\langle\Gamma_\gamma\rangle$ was available, then that $\langle\Gamma_\gamma\rangle$ would be assigned for the radiation width. The sixth column in Table IV, labeled Γ_γ source, designates whether the Γ_γ in the table was fitted from the data (FIT), fixed to an average value (AVG), or fixed to the ENDF/B-VII.0 value (ENDF).

The $\langle\Gamma_\gamma\rangle$ and $\Delta\langle\Gamma_\gamma\rangle$ values that are cited throughout Table IV whenever "AVG" appears in the "Γ_γ source" column are presented in Table VI. They were determined from measured resonances that were sensitive to the value of the radiation width. They were determined from resonances meeting the three criteria and applied to those that did not meet the criteria. The $\Delta\langle\Gamma_\gamma\rangle$ values listed in Table VI were defined as the standard deviation of the distribution of SAMMY-fitted radiation widths for resonances of a particular isotope, orbital angular momentum, and spin, which met the three criteria listed above. As noted in Table VI, some of the $\langle\Gamma_\gamma\rangle$ values came from a single resonance. The lone s-wave resonance in ^{96}Mo occurs at 131 eV. This resonance is very distinct in many sample thicknesses as shown in Fig. 2. Therefore, the $\Delta\Gamma_\gamma$ for this resonance is very small, 1 meV. There were no p-wave data that were sensitive to the value of radiation width for ^{94}Mo, ^{95}Mo, ^{96}Mo, and ^{97}Mo. For ^{94}Mo, ^{95}Mo, and ^{97}Mo, the p-wave $\Delta\langle\Gamma_\gamma\rangle$ was assumed to be the same as the s-wave $\Delta\langle\Gamma_\gamma\rangle$ when assigning $\Delta\Gamma_\gamma$ values in Table IV.

IV.G. Isotopic Differences in Capture Detector Efficiency

In neutron capture measurements, the efficiency of the detector system is different for each isotope. Preliminary resonance parameter fits were performed with the assumption of equal efficiency for each isotope. After

TABLE VI

Measured Average Γ_γ and Their Uncertainties for Molybdenum

Isotope	Angular Momentum and Spin	Average Γ_γ (meV)	Uncertainty in Γ_γ (meV)	Comment
92	All	Unknown	Unknown	No data
94	s	140	60	Single resonance at 1542 eV
95	s 2^+	180	10	Based primarily on 554-eV resonance
	s 3^+	170	40	Based primarily on 45- and 358-eV resonances
96	s	85	1	Single resonance at 131 eV
97	s 2^+	140	20	Based primarily on 286- and 505-eV resonances
	s 3^+	120	30	Based primarily on 397- and 558-eV resonances
98	s	89	1	Based on 467-eV resonance
	p $\frac{1}{2}$-	110	10	Two resonances at 429 and 612 eV
	p $\frac{3}{2}$-	120	30	Single resonance at 818 eV
100	s	56	1	Based primarily on 364-eV resonance
	p $\frac{1}{2}$-	90	50	Single resonance at 1768 eV
	p $\frac{3}{2}$-	69	7	Based primarily on 1697-eV resonance

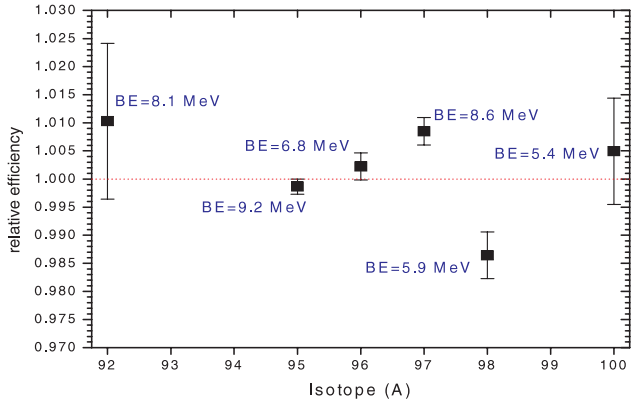

Fig. 7. Relative capture detector efficiencies for the molybdenum isotopes. The neutron separation energy, or binding energy (BE), of a neutron in each isotope is noted. One would expect higher efficiency when more gamma energy is available for detection. The error bars come from the SAMMY calculation.

TABLE VII

Resonance Integrals for the Molybdenum Isotopes in Barns*

Molybdenum Isotope	ENDF/B-VII	RPI	Percent Change (%)
92	0.968	0.95 ± 0.01	−2
94	1.46	1.37 ± 0.09	−6
95	110	121 ± 1	+10
96	17.5	17.07 ± 0.06	−2
97	17.5	16.0 ± 0.7	−9
98	6.56	6.39 ± 0.05	−3
100	3.85	3.44 ± 0.03	−11

*The RPI values were calculated from the measured resonance parameters shown in Table IV using the NJOY (Ref. 20) and INTER (Ref. 21) programs. The uncertainties in resonance integrals were calculated using resonance parameter uncertainties from Table IV and the method of Barry.[13] The percent change of RPI relative to ENDF/B-VII.0 is also presented.

capture flux normalization was determined by the iterative process described in Sec. IV.D, a subsequent normalization was done near strong, isolated resonances for a particular molybdenum isotope to obtain isotope-specific relative capture efficiencies. The resulting relative capture detector efficiencies are shown in Fig. 7. The error bars shown in Fig. 7 came from the SAMMY calculations. These efficiencies were used in the SAMMY fits of final resonance parameters shown in Table IV.

The neutron separation energy, or binding energy, of a neutron in each isotope is noted on Fig. 7. Higher binding energy implies more gamma energy available for detection. There is no clear trend of efficiency with binding energy. But, three of the four isotopes with binding energy >6.0 MeV lie above 1.0 relative efficiency while one of two isotopes with binding energy <6.0 MeV lies below 1.0.

IV.H. Resonance Integrals

Infinitely dilute capture resonance integrals (*RI*s) have been calculated from Eq. (4):

$$RI = \int_{0.5\ \mathrm{eV}}^{20\ \mathrm{MeV}} \sigma_\gamma(E)\,\frac{dE}{E}\ , \qquad (4)$$

where

$\sigma_\gamma(E)$ = capture cross section in barns, Doppler broadened to 293 K

E = energy (eV).

The cross section was calculated from the resonance parameters shown in Table IV. Above 2 keV ENDF/B-VII.0 cross sections were used. The resonance integrals were calculated using the NJOY (Ref. 20) and INTER (Ref. 21) programs. The results are shown in Table VII in units of barns. For six of seven isotopes the resonance integral is smaller than ENDF's. The exception was ^{95}Mo, whose resonance integral was measured as 10% larger than ENDF. Molybdenum-95 and ^{97}Mo were the isotopes containing the most resonances. The largest reductions relative to ENDF were 9% in ^{97}Mo and 11% in ^{100}Mo. The number of resonances in each isotope is shown in Table I. The uncertainty in the resonance integrals was calculated by differentiating *RI* with respect to resonance parameters according to the error propagation formula and treating $\sigma_\gamma(E)$ as a sum of single-level Breit-Wigner resonances.[13]

IV.I. Statistical Properties of the Resonance Parameters

All measurements were made with natural samples, so all isotope assignments were taken from ENDF/B-VII. Therefore, there is no additional information in this measurement regarding average level spacing.

Statistical distributions of reduced neutron widths were investigated for the two isotopes with the most resonances, ^{95}Mo and ^{97}Mo. The reduced neutron widths were divided by the unweighted average reduced neutron width for each isotope and J value. These unitless ratios for both J values in ^{95}Mo and ^{97}Mo were plotted as a cumulative distribution in Fig. 8 and compared to a χ^2 distribution with one degree of freedom, i.e., the Porter-Thomas distribution. ENDF/B-VII neutron widths were processed in the same way and also plotted on Fig. 8. Three observations were made regarding the neutron width distributions as follows:

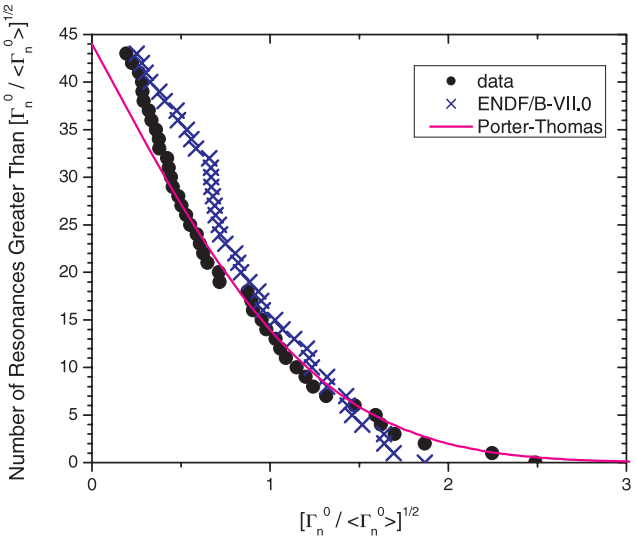

Fig. 8. Cumulative distribution of reduced neutron widths for ^{95}Mo and ^{97}Mo, a combined total of 44 resonances. Each reduced neutron width has been divided by an unweighted average reduced neutron width, $\langle\Gamma_n^0\rangle$ specific to its isotope and J value. The solid curve is the expected Porter-Thomas distribution based on 44 resonances. The RPI neutron widths match the theory above an ordinate of 0.45.

1. The RPI neutron widths are a better match to the theory of a Porter-Thomas distribution than those of ENDF.

2. According to the theory several s-wave resonances exist but are not observable below our minimum measurable width.

3. If about four of the weakest s-wave resonances are actually misassigned p-waves, the data with small neutron widths would fall on the Porter-Thomas curve.

Neutron strength functions S_0 were measured for the two isotopes with the most resonances, ^{95}Mo and ^{97}Mo. The measured values are compared to those of ENDF/B-VII.0 and the *Atlas of Neutron Resonances*[22] in Table VIII. The RPI values were determined from 18 resonances in ^{95}Mo and 26 resonances in ^{97}Mo. The uncertainty given in Table VIII was based on a quadrature sum of the SAMMY-propagated uncertainties given in Table IV. The neutron strength for the two odd-mass nuclei with the same Jπ are within statistics of each other. However, the two references do not show such a similarity between the ^{95}Mo and ^{97}Mo nuclei. The strength function for ^{97}Mo is larger than that of ENDF/B-VII.0 primarily because of the observation of two resonances, 1249.6 eV shown in Fig. 5 and 1534.8 eV shown in Fig. 6, which are much stronger than suggested by ENDF. In Fig. 5 the two ENDF curves correspond to the 6.35-mm Mo thickness. Yet the ENDF curves lie closer to the thin sample data near the 1249.6-eV resonance. The 6.35-mm Mo data and the corresponding SAMMY fit display a larger neutron width, which contributes to the larger ^{97}Mo neutron strength function shown in Table VIII. The curves in Fig. 6 lead to a similar observation. There are three resonances between 1525 and 1545 eV. The SAMMY curve is a much better fit to the data than ENDF because the middle resonance at 1534.8 eV is much stronger relative to ENDF. This resonance also contributes to the larger ^{97}Mo neutron strength function shown in Table VIII.

TABLE VIII

Neutron Strength Function, S_0, for the Two Isotopes with the Most Resonances, ^{95}Mo and ^{97}Mo*

	S_0 ^{95}Mo	S_0 ^{97}Mo
RPI	0.436 ± 0.009[a]	0.438 ± 0.005[a]
ENDF/B-VII	0.45	0.37
Atlas of Neutron Resonances[22]	0.47 ± 0.17	0.33 ± 0.08

*The RPI values are the present measurements of 18 ^{95}Mo resonances and 26 ^{97}Mo resonances. The ENDF/B-VII value is from the header block of the online data file and does not include uncertainties. The units of strength function are $10^{-4} \times \text{meV}^{-(1/2)}$.

[a]The uncertainty is a quadrature sum of the SAMMY-propagated errors given in Table IV.

Statistical distributions of radiation widths were investigated for the two isotopes with the most resonances, ^{95}Mo and ^{97}Mo. The cumulative distribution is shown in Fig. 9. Only resonance data sensitive to the value of Γ_γ, based on the criteria of Sec. IV.F, were included in the analysis. The radiation widths were divided by the weighted average radiation width for each isotope allowing data from the two isotopes to be combined. The weighting factors were determined from the uncertainties listed in Table IV. These unitless radiation width-to-average ratios were compared to χ^2 distributions with various degrees of freedom. The best fit was a χ^2 distribution with 67 degrees of freedom. The data agree reasonably well with the theory for multiple exit channels. ENDF/B-VII.0 radiation widths for the same resonances are also plotted on Fig. 9. The average radiation widths for each isotope used to process the ENDF/B-VII.0 values were unweighted since no uncertainty information is provided in ENDF. The best-fit cumulative χ^2 distribution to their values had 129 degrees of freedom.

IV.J. Components of Resonance Parameter Uncertainties

The components of resonance parameter uncertainty were background, capture flux normalization, resolution function, time zero, sample thickness, burst width, flight path length, and isotopic differences in capture detector

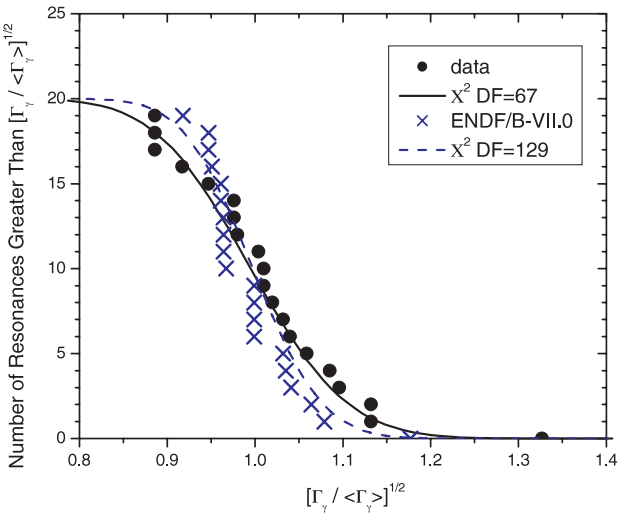

Fig. 9. Cumulative distribution of radiation widths for resonances in ^{95}Mo and ^{97}Mo whose data were sensitive to the value of Γ_γ . There were 11 such resonances in ^{95}Mo and 9 in ^{97}Mo. Each Γ_γ value was divided by the weighted average value for that isotope allowing data from the two isotopes to be combined. The data are plotted as the square root of these ratios in order to make the plot more compact. The solid curve is the best fit to the data cumulative χ^2 distribution with 67 degrees of freedom. The dashed curve is the best fit to ENDF/B-VII.0 cumulative χ^2 distribution with 129 degrees of freedom.

efficiency. They were propagated into resonance energy and neutron width uncertainties through use of the Propagated Uncertainty Parameters (PUP) feature in SAMMY (Ref. 5). Radiative widths were treated in the same way whenever the ratio of capture-to-scattering Γ_γ / Γ_n was <5. The determination of radiative widths and their uncertainties was described in Sec. IV.F. The resulting resonance parameter uncertainties are given in Table IV.

The uncertainty in transmission background was derived from molybdenum and uranium data in saturated resonances. The uncertainty in capture background was due, in part, to quantifying the activation of NaI from scattered neutrons.

The capture flux normalization was based on molybdenum fits to transmission data in an iterative process described in Sec. IV.D. The uncertainty in the flux normalization that was propagated in the resonance parameters was based on the convergence criterion of that process.

The resolution function parameters used in SAMMY to analyze the 2004 molybdenum transmission data were fitted to uranium transmission data included in the same measurement (Sec. IV.E). The uncertainties in the resolution parameters from that fit were propagated into the subsequent resonance parameter fits to the 2004 molybdenum transmission data. The uncertainties in the resolution function parameters for 1995 capture and transmission measurements were taken from an earlier evaluation.[19]

The time zero values were derived from the 2004 uranium transmission data. The uncertainties in the time zero values that were propagated into the subsequent resonance parameter fits were based on comparisons to measurements of the gamma burst produced at the beginning of each LINAC pulse. The flight path lengths were based on fits to uranium resonances. The uncertainty in the flight path length propagated through to the resonance parameters was based on the differences between the two uranium samples, the SAMMY error on each fit, and the difference from previously fitted values for the same experimental configuration.

Sample thickness uncertainties are given in Table III. They were propagated into the final resonance parameters. Measurements of the gamma burst produced at the beginning of each LINAC pulse were fit with a Gaussian to determine the width and uncertainty in the width of the burst in units of time. Isotopic differences in capture detector efficiency were discussed in Sec. IV.G. The uncertainties used in the analysis of resonance parameters came directly from the SAMMY fits.

V. DISCUSSION AND CONCLUSIONS

Transmission and capture data were measured and analyzed. Resonance parameters of elemental molybdenum were extracted. The original features of this measurement and analysis were in its treatment of radiation widths, their uncertainties, and uncertainties in general. This measurement establishes a state-of-the-art refinement of the resonance parameters given in ENDF/B-VII.0. SAMMY fits to multiple data sets and sample thicknesses from a single set of resonance parameters are shown in Figs. 2 through 6. The uncertainties in the resonance parameters of many of the larger resonances have been improved compared to Ref. 22. In the energy region between 10 and 600 eV, where transmission and capture data were taken, the uncertainties of the resonance parameters of five of the strongest resonances (44.6, 131, 358, 363, and 467 eV) were reduced compared to Ref. 22. For the four strong resonances at 681, 1526, 1535, and 1542 eV (see Fig. 6), uncertainties in the neutron widths were reduced compared to Ref. 22. Above 600 eV, where only transmission data were available, uncertainties in radiative widths were not reduced compared to Ref. 22. But, the current estimates of radiation width uncertainties were based upon the conservative method described in Sec. IV.F. This method addressed the issue of insensitivity of transmission data to radiation widths. Rather than relying on fitted results to data that contained very little radiation width information, a method was developed to determine accurate radiation

widths of a few sensitive resonances where measured radiation width information was found in the data. These data determined average radiation widths that were then assigned to the insensitive resonances. A distribution of radiation widths was determined for each isotope, and where data were available, for each orbital angular momentum and spin (total angular momentum); see Table VI. The standard deviation of each distribution was used as the uncertainty on the average radiation width.

The determination of experimental background is a crucial task in any resonance parameter analysis. Molybdenum and uranium samples thick enough to provide several saturated resonances gave detailed information about the background in each measurement. A fixed sodium notch was used to provide a definitive background point near the maximum energy of this analysis.

A proper definition of the resolution function was another critical component of the accurate determination of resonance parameters. The uranium data provided valuable information about the resolution function in transmission. A time-dependent exponential tail component of the transmission resolution function was implemented in the SAMMY analysis.

This detailed uncertainty information for background, resolution function, etc., was used with the PUP feature of the SAMMY code to propagate all known sources of uncertainty into the final results.

Reductions in resonance integrals were observed when compared to ENDF/B-VII.0 for six of the seven stable isotopes. The largest reductions were 9% in ^{97}Mo and 11% in ^{100}Mo. The one isotope whose resonance integral was found to be larger than ENDF was significant; the ^{95}Mo resonance integral was 10% larger than that of ENDF/B-VII.0.

The distributions of reduced neutron widths for ^{95}Mo and ^{97}Mo were compared to those of ENDF/B-VII.0 and to the theoretical Porter-Thomas distribution. Several very weak resonances are expected to exist that have not been identified by the present measurements or by ENDF/B-VII.0. If a few of the weaker resonances were p-waves rather than s-waves, the agreement with the Porter-Thomas distribution of level widths would improve.

Neutron strength functions for ^{95}Mo and ^{97}Mo were measured and compared to ENDF/B-VII.0 and Mughabghab.[22] The strength of ^{95}Mo and ^{97}Mo are within uncertainties of each other. This agrees with our intuition that two isotopes with odd-mass and the same $J\pi$ should have similar neutron strengths. However, it represents a departure from ENDF/B-VII.0 and Mughabghab[22] in which ^{97}Mo has a significantly smaller strength. Two resonances are most responsible for the larger ^{97}Mo neutron strength, those at 1249.6 and 1534.8 eV.

The cumulative distribution of radiation widths for ^{95}Mo and ^{97}Mo were compared to those of ENDF/B-VII.0 and to the χ^2 distribution. Only those resonances whose measured data contained radiation width information were included in the distribution. The best fit to these data was a χ^2 distribution with 67 degrees of freedom. The best-fit χ^2 distribution to the ENDF/B-VII.0 distribution of radiation widths for the same resonances had 129 degrees of freedom.

REFERENCES

1. H. WEIGMANN, G. ROHR, and J. WINTER, "Neutron Capture Measurements and Resonance Parameters of Mo-Isotopes," *Nucl. Phys. A*, **104**, 513 (1967).

2. S. WYNCHANK, J. GARG, W. HAVENS, and J. RAINWATER, "Neutron Resonance Spectroscopy. VI. Mo, Sb, Te, Pr," *Phys. Rev.*, **166**, 4 (1968).

3. A. R. DEL. MUSGROVE, B. J. ALLEN, J. W. BOLDEMAN, and R. L. MACKLIN, "Average Neutron Resonance Parameters and Radiative Capture Cross Sections for the Isotopes of Molybdenum," *Nucl. Phys. A*, **270**, 108 (1976).

4. O. A. WASSON, B. J. ALLEN, R. R. WINTERS, R. L. MACKLIN, and J. A. HARVEY, "Neutron Resonance Parameters of ^{92}Mo," *Phys. Rev. C*, **7**, 4 (1973).

5. N. M. LARSON, "Updated Users' Guide for SAMMY: Multilevel R-Matrix Fits to Neutron Data Using Bayes' Equations," ORNL/TM-9179/R5, Lockheed Martin Energy Research Corporation, Oak Ridge National Laboratory (2000).

6. M. B. CHADWICK et al., "ENDF/B-VII.0: Next Generation Evaluated Nuclear Data Library for Science and Technology," *Nucl. Data Sheets*, **107**, *12*, 2931 (2006).

7. R. E. SLOVACEK, R. C. BLOCK, Y. DANON, C. WERNER, G.-U. YOUK, J. A. BURKE, N. J. DRINDAK, F. FEINER, J. A. HELM, and K. W. SEEMANN, "Neutron Cross-Section Measurements at the Rensselaer LINAC," *Proc. Topl. Mtg. Advances in Reactor Physics*, Knoxville, Tennessee, April 11–15, 1994, American Nuclear Society (1994).

8. R. C. BLOCK, P. J. MARANO, N. J. DRINDAK, F. FEINER, K. W. SEEMANN, and R. E. SLOVACEK, "A Multiplicity Detector for Accurate Low-Energy Neutron Capture Measurements," *Proc. Int. Conf. Nuclear Data for Science and Technology*, Mito, Japan, May 30–June 3,1988, p. 383 (1988).

9. R. C. BLOCK, Y. DANON, C. J. WERNER, G. YOUK, J. A. BURKE, N. J. DRINDAK, F. FEINER, J. A. HELM, J. C. SAYRES, and K. W. SEEMANN, "Neutron Time-of-Flight Measurements at the Rensselaer LINAC," *Proc. Int. Conf. Nuclear Data for Science and Technology*, Gatlinburg, Tennessee, May 9–13, 1994, Vol. 1, p. 81, American Nuclear Society (1994).

10. R. W. HOCKENBURY, Z. M. BARTOLOME, J. R. TATARCZUK, W. R. MOYER, and R. C. BLOCK, *Phys. Rev.*, **178**, *4*, 1746 (1969).

11. M. E. OVERBERG, B. E. MORETTI, R. E. SLOVACEK, and R. C. BLOCK, "Photoneutron Target Development for the

RPI Linear Accelerator," *Nucl. Instrum. Methods Phys. Res. A*, **438**, 253 (1999).

12. G. LEINWEBER, "Analysis of Moxon-Rae and Multiplicity Detectors Using Monte Carlo Techniques," MS Thesis, Rensselaer Polytechnic Institute (1989).

13. D. P. BARRY, "Neodymium Neutron Transmission and Capture Measurements and Development of a New Transmission Detector," PhD Thesis, Rensselaer Polytechnic Institute (2003).

14. B. E. MORETTI, "Molybdenum Neutron Transmission Measurements and the Development of an Enhanced Resolution Neutron Target," PhD Thesis, Rensselaer Polytechnic Institute (1996).

15. Y. DANON and R. C. BLOCK, *Nucl. Instrum. Methods Phys. Res. A*, **485**, 585 (2002).

16. G. LEINWEBER, J. A. BURKE, H. D. KNOX, N. J. DRINDAK, D. W. MESH, W. T. HAINES, R. V. BALLAD, R. C. BLOCK, R. E. SLOVACEK, C. J. WERNER, M. J. TRBOVICH, D. P. BARRY, and T. SATO, "Neutron Capture and Transmission Measurements and Resonance Parameter Analysis of Samarium," *Nucl. Sci. Eng.*, **142**, 1 (2002).

17. G. LEINWEBER, J. BURKE, C. R. LUBITZ, H. D. KNOX, N. J. DRINDAK, R. C. BLOCK, R. E. SLOVACEK, C. J. WERNER, N. C. FRANCIS, Y. DANON, and B. E. MORETTI, "Neutron Capture and Total Cross-Section Measurements and Resonance Parameter Analysis of Zirconium up to 2.5 keV," *Nucl. Sci. Eng.*, **134**, 50 (2000).

18. A. SOVITZKY and M. J. E. GOLAY, "Smoothing and Differentiation of Data by Simplified Least Squares Procedures," *Anal. Chem.*, **36**, 1627 (1964).

19. M. J. TRBOVICH, "Hafnium Neutron Cross Sections and Resonance Analysis," PhD Thesis, Rensselaer Polytechnic Institute (2003).

20. R. E. MacFARLANE and D. W. MUIR, "The NJOY Nuclear Data Processing System Version 91," LA-12740-M, Los Alamos National Laboratory (1994).

21. C. L. DUNFORD, "ENDF Utility Codes Release 7.01/02," USCD1212/07 (Apr. 27, 2005).

22. S. F. MUGHABGHAB, *Atlas of Neutron Resonances*, 5th ed., Elsevier, New York (2006).